

# Treatment of Amoxicillin Antibiotic from the Surface Water using Carboxymethyl Tragacanth Gum-Grafted-Polyaniline Doped to Fe<sub>2</sub>O<sub>3</sub> Bionanocomposites

Oztekin R and Sponza DT\*

Dokuz Eylül University, Engineering Faculty, Department of Environmental Engineering, Tınaztepe Campus, Turkey

## \*Corresponding author:

Delia Teresa Sponza, Dokuz Eylül University, Engineering Faculty, Department of Environmental Engineering, Tınaztepe Campus, 35160 Buca/Izmir, Turkey

Received: 19 May 2023

Accepted: 26 June 2023

Published: 04 July 2023

J Short Name: AJSCCR

## Copyright:

©2023 Sponza DT, This is an open access article distributed under the terms of the Creative Commons Attribution License, which permits unrestricted use, distribution, and build upon your work non-commercially.

## Keywords:

ANOVA statistical analysis; Amoxicillin; Antibiotics; Brunauer–Emmet–Teller (BET); Carboxymethyl tragacanth gum-grafted-polyaniline/Fe<sub>2</sub>O<sub>3</sub> bionanocomposite; Cost analysis; Dubinin–Astakhov (DA) method; Energy-dispersive X-ray (EDX); Field emission scanning electron microscopy (FESEM); Fourier transform infrared spectroscopy (FTIR); Micropollutants; Pharmaceutical industry wastewater; Thermal gravimetric analysis (TGA); Transmission Electron Microscopy (TEM); Value stream mapping (VSM); X-Ray Diffraction (XRD)

## Citation:

Sponza DT. Treatment of Amoxicillin Antibiotic from the Surface Water using Carboxymethyl Tragacanth Gum-Grafted-Polyaniline Doped to Fe<sub>2</sub>O<sub>3</sub> Bionanocomposites. *Ame J Surg Clin Case Rep.* 2023; 6(13): 1-17

## 1. Abstract

In the present study, treatment of amoxicillin (AMX) antibiotic from the surface water using carboxymethyl tragacanth gum-grafted-polyaniline doped to Fe<sub>2</sub>O<sub>3</sub> (CMTG-g-PANI/Fe<sub>2</sub>O<sub>3</sub>) bionanocomposites (BNCs) was examined with adsorption process from pharmaceutical industry wastewater (PI ww) plant, İzmir, Turkey. Different pH values (4.0, 5.0, 7.0 and 9.0), increasing adsorption times (5 min, 10 min, 20 min and 40 min), increasing AMX concentrations (100 mg/l, 200 mg/l, 300 mg/l, 400 mg/l and 500 mg/l), increasing CMTG-g-PANI/Fe<sub>2</sub>O<sub>3</sub> BNCs concentrations (5 mg/l, 15 mg/l, 30 mg/l and 45 mg/l), respectively, was operated during adsorption process in the efficient removals of AMX micropollutants in PI ww. The characteristics of the synthesized NPs were assessed using XRD, EDX, FESEM, FTIR, TEM and VSM analyses, respectively. Also, thermal gravimetric analysis (TGA) was operated with Brunauer–Emmet–Teller (BET) measurements by a multi-point method, and the pore parameters were calculated via the Dubinin–Astakhov (DA) method. ANOVA statistical analysis was used for all experimental samples. The maximum 99.36% AMX removal was obtained during adsorption process in PI ww at pH=7.0 and at 25°C. The maximum 99.07% AMX removal was observed during adsorption process in PI ww after 20 min, at pH=7.0 and at 25°C, respectively. The maximum 99.23% AMX removal was found with adsorption process in PI ww, at

100 mg/l AMX, after 20 min, at pH=7.0 and at 25°C, respectively. The maximum 99.20% AMX removal was measured to 5 mg/l CMTG-g-PANI/Fe<sub>2</sub>O<sub>3</sub> BNCs with adsorption process in PI ww, at 100 mg/l AMX after 20 min, at pH=7.0 and at 25°C, respectively. The maximum 99% and 99% AMX recovery efficiencies were measured in PI ww during adsorption process, after 1. recycle time and 2. recycle time, respectively, at 100 mg/l AMX after 20 min, at pH=7.0 and at 25°C, respectively. A granular structure with good thermal stability (34wt% char yield), 8.1143 m<sup>2</sup>/g specific surface area and 23 emu/g magnetization saturation were measured for CMTG-g-PANI/Fe<sub>2</sub>O<sub>3</sub> BNCs. 983.11 mg/g maximum adsorption capacity was observed at pH=7.0, at 20 min adsorption mixing time, at 5 mg/l CMTG-g-PANI/Fe<sub>2</sub>O<sub>3</sub> BNCs, at 500 mg/l initial AMX concentration, respectively. The Freundlich isotherm model and the pseudo-second-order kinetic models are much more suitable with the experimental data for AMX removal in PI ww during adsorption process with CMTG-g-PANI/Fe<sub>2</sub>O<sub>3</sub> BNCs. The adsorption/desorption process showed that CMTG-g-PANI/Fe<sub>2</sub>O<sub>3</sub> BNCs could continue to remove AMX after three sequential adsorption/desorption cycles without significantly losing adsorption capacity. Finally, the combination of a simple, easy operation preparation process, excellent performance and cost effective, makes this CMTG-g-PANI/Fe<sub>2</sub>O<sub>3</sub> BNCs bioadsorbent a promising option during adsorption process in PI ww treatment.

## 2. Introduction

Emerging contaminants (ECs), sometimes known as contaminants of emerging concern (CECs) can refer to a wide variety of artificial or naturally occurring chemicals or materials that are harmful to human health after long-term disclosure. ECs can be classified into several classes, including agricultural contaminants (pesticides and fertilizers), medicines and antidote drugs, industrial and consumer waste products, and personal care and household cleaning products [1, 2]. Antibiotics are one of the ECs that have raised concerns in the previous two decades because they have been routinely and widely used in human and animal health care, resulting in widespread antibiotic residues discharged in surface, groundwater, and wastewater.

Antibiotics, which are widely utilized in medicine, poultry farming and food processing [3, 4], have attracted considerable attention due to their abuse and their harmful effects on human health and the ecological environment [5, 6]. The misuse of antibiotics induces Deoxyribonucleic Acid (DNA) contamination and accelerates the generation of drug-resistant bacteria and super-bacteria [7-9]; thus, some diseases are more difficult to cure [10]. A number of studies have revealed that the level of antibiotics in the soil, air and surface water and even in potable water, is excessive in many areas [11-13], which will ultimately accumulate in the human body via drinking water and then damage the body's nervous system, kidneys and blood system. Therefore, it is necessary to develop an efficient method to remove antibiotics present in PI ww.

The uncontrolled, ever-growing accumulation of antibiotics and their residues in the environment is an acute modern problem. Their presence in water and soil is a potential hazard to the environment, humans, and other living beings. Many therapeutic agents are not completely metabolized, which leads to the penetration of active drug molecules into the biological environment, the emergence of new contamination sources, the wide spread of bacteria and microorganisms with multidrug resistance [14-16]. Modern pharmaceutical wastewater facilities do not allow efficient removal of antibiotic residues from the environment [17, 18], which leads to their accumulation in ecological systems [19, 20]. Global studies of river pollution with antibiotics have shown that 65% of surveyed rivers in 72 countries on 6 continents are contaminated with antibiotics [21]. According to the World Health Organization (WHO), surface and groundwater, as well as partially treated water, containing antibiotics residue and other pharmaceuticals, typically at < 100 ng/l concentrations, whereas treated water has < 50 ng/l concentrations, respectively [22]. However, the discovery of ECs in numerous natural freshwater sources worldwide is growing yearly. Several antibiotic residues have been reported to have been traced at concentrations greater than their ecotoxicity endpoints in the marine environment, specifically in Europe and Africa [23]. Thus, the European Union's Water Framework Directive enumerated certain antibiotics as priority contaminants [24-26]. In

some rivers, the concentrations were so high that they posed a real danger to both the ecosystem and human health. This matter, the development of effective approaches to the removal of antibiotics from the aquatic environment is of great importance.

More than 90% of medications taken orally do not decompose, thus they become active compounds. Since antibiotics are highly soluble in water, conventional treatment procedures cannot eliminate them, which poses a significant obstacle to their removal [27]. The removal of antibiotics and their residues from water and wastewater prior to their final release into the environment is of particular concern [28]. Modern purification methods can be roughly divided into the following three categories depending on the purification mechanism: biological treatment [29, 30], chemical degradation [28, 31], and physical removal. Each of these methods has its own advantages and disadvantages. For example, biological purification can remove most antibiotic residues, but the introduction of active organisms into the aquatic environment can upset the ecological balance. Various chemical approaches (ozonation, chlorination, and Fenton oxidation) cannot provide complete purification and, in some cases, lead to the death of beneficial microorganisms due to low selectivity.

The most common techniques for removing antibiotics include electrochemical degradation [32], Fenton oxidation process [33], UV radiation [34, 35], ozonation [36], membrane filtration [37, 38], photolysis [39], biological degradation [40], and adsorption [41]. The most appealing technology, nevertheless, is the adsorption process, which has a flexible and straightforward design, is simple to use, is inexpensive, and is highly effective [42, 43]. The adsorbent used in industrial applications should be able to quickly absorb the target material and be ecologically benign [44].

Amoxicillin (AMX) is one of the most widely employed commercial penicillins and based on a  $\beta$ -lactam antibiotic categorized as penicillin [45], due to its high bacterial resistance and large spectrum against a wide range of microorganisms [46, 47]. Systemic, bacterial, and gastrointestinal illnesses are treated with AMX in both human and veterinary medicine. It is widely recognized that AMX is utilized in modern medicine, and its ecotoxicity contributes to the danger of medical wastewater. It can be found in medical wastewater coming from pharmaceutical plants and hospitals, which causes skin disorders and microbial resistance among pathogen organisms. Due to the difficulty of breaking down this antibiotic, the residue is eliminated in the urine and feces. Consuming too much AMX creates resistant bacteria because it accumulates in the body and feeds the organisms [48]. It has been reported that about 30–90% of AMX are discharged into the environment through human and animal excrements [49], and the presence of AMX in the ng/l to mg/l concentration ranges in surface water, domestic and industrial wastewater. Since resistant bacteria can cause diseases that are not treatable with traditional antibiotics, AMX waste must be treated before its disposal [50]. It is essential

to use an effective technique to remove AMX before it is released into the aquatic environment.

Several methods have been reported for removal of AMX in different matrices. These include electrodegradation [51], advanced oxidation [52], photocatalytic degradation [53], and adsorption [49, 54-56], among others. Adsorption process has been found to more effective for removal of AMX because it restricts the transportation of pollutants into water systems [57]. Also, adsorption process is attractive because it uses different adsorbents. These include activated carbon (AC) [49, 54], carbon nanotubes [47, 57, 58], magnetic  $\text{Fe}_3\text{O}_4$ /activated carbon nanocomposite (NCs) [59, 60], magnetic graphene oxide [55, 56], and porous polymers [61]. In order to effectively remove AMX from water, a range of micro/nanostructures were deemed acceptable adsorbents, either as single phases or composites. The use of various adsorbents for AMX removal from aqueous solutions were reported at literature. A metal-organic framework (MIL-53(Al)) was prepared with a hydrothermal technique and used as an adsorbent for the removal of AMX from surface water [62]. 758.5 mg/g MIL-53 adsorption capacity in experimental conditions due to its high surface area. An adsorbent based on  $\text{NH}_4\text{Cl}$ -induced AC was employed for the removal of AMX from water. 99% AMX removal was measured, owing to the high specific surface area ( $1029 \text{ m}^2/\text{g}$ ) of  $\text{NH}_4\text{Cl}$ -induced AC [63]. 97.9% AMX removal from surface water was reported by an adsorbent based on AC produced from pomegranate peel/iron nanoparticles, at  $\text{pH}=5.0$  after 30 min contact time [64]. A green magnetic adsorbent based on functional  $\text{CoFe}_2\text{O}_4$ -modified biochar was used for AMX removal from surface water. The maximum 99.99 mg/g adsorption capacity is obtained at  $\text{pH}=7.0$  and at  $25^\circ\text{C}$  [65].

Tragacanth gum (TG), as a colorless and odorless natural polymer, is a highly complex heterogeneous anionic polysaccharide that forms from the stems and branches of *Astragalus gummier* and other Asian *Astragalus* species [66]. Within a few weeks, the exudate can be recovered after it has solidified into flakes or coils of ribbon [67]. TG is a substance that is found in Turkey, Iran, India and Afghanistan. Neutral and anionic sugars, such as D-galacturonic acid, D-galactose, D-xylose, L-arabinose, L-fucose, and d-glucose are found in TG [66, 68]. TG natural polymer is utilized in a broad range of areas, including the food, pharmaceutical, cosmetic [69], textile, printing, and leather industries [66, 70-76]. It is possible because of its amazing qualities, including (i) superior acid, heat, and enzyme resistance; (ii) longer shelf life and microbial resistance; (iii) non-toxicity, non-allergenicity, non-carcinogenicity, non-mutagenicity, and non-teratogenicity; (iv) biocompatibility; and (v) biodegradability [66, 70-76]. In addition to, TG is inexpensive, readily accessible, and has great solubility, strong thermal stability, and a long shelf life [77]. In TG, hydroxyl- and carboxylic-acid-reactive functional groups can be used

for chelation in removing pollutants from surface water. In order to increase the adsorption capacity of natural polymers, copolymerization with functional monomers and inorganic fillers are added. The nanoparticles (NPs) synthesis mediated by gum TC qualifies various principles of green chemistry such as (i) natural availability/renewability, (ii) non-toxicity/inherently safer, (iii) aqueous solubility, (iv) dual functional role of reducer and stabilizer, and (v) biodegradability [71, 74, 78].

Iron (III) oxide ( $\text{Fe}_2\text{O}_3$ , hematite or red iron oxide) is an inorganic compound. It occurs naturally in rocks of all ages. It appears as a red-brown solid. It is odourless and  $\text{pH}=7.0$  [79].  $\text{Fe}_2\text{O}_3$  NPs is used as a feedstock in the production of iron, as a pigment (Pigment Brown 6, Pigment Red 101), in cosmetics, in dental composites, an important ingredient in calamine lotion, to apply the final polish on metallic jewellery, in magnetic disk and magnetic tapes, and in pharmaceuticals industry [79]. If  $\text{Fe}_2\text{O}_3$  NPs is inhaled, iron causes irritation of the gastrointestinal tract and lungs [79].

In this study, treatment of AMX antibiotic from the surface water using CMTG-g-PANI/ $\text{Fe}_2\text{O}_3$  BNCs was examined with adsorption process from PI ww plant, İzmir, Turkey. Different pH values (4.0, 5.0, 7.0 and 9.0), increasing adsorption times (5 min, 10 min, 20 min and 40 min), increasing AMX concentrations (100 mg/l, 200 mg/l, 300 mg/l, 400 mg/l and 500 mg/l), increasing CMTG-g-PANI/ $\text{Fe}_2\text{O}_3$  BNCs concentrations (5 mg/l, 15 mg/l, 30 mg/l and 45 mg/l), respectively, was operated during adsorption process in the efficient removals of AMX micropollutants in PI ww. Also, increasing recycle times (Between 1 and 20 cycle) was examined for the AMX removal. The characteristics of the synthesized NPs were assessed using XRD, EDX, FESEM, FTIR, TEM and VSM analyses, respectively. In addition to, TGA analysis was operated with BET measurements by a multi-point method, and the pore parameters were calculated via the Dubinin-Astakhov (DA) method. ANOVA statistical analysis was used for all experimental samples.

### 3. Materials and Methods

#### 3.1. Characterization of Pharmaceutical Industry Wastewater

Characterization of the biological aerobic activated sludge process from a PI ww plant, İzmir, Turkey was performed. The results are given as the mean value of triplicate samplings (Table 1).

#### 3.2. Experimental Chemicals

$\text{Na}_2\text{HPO}_4$ , NaCl,  $\text{KH}_2\text{PO}_4$  and  $\text{NH}_4\text{Cl}$  purchased from Merck (Merck, Germany). The KOH tablets used as electrolyte was purchased from Merck (Merck, Germany). TG with high-quality in translucent flakes was purchased from Sigma-Aldrich (Germany). The specific surface area of the samples was studied by the Brunauer-Emmett-Teller (BET) technique according to Belsorp mini II, MicrotracBEL, Osaka, Japan. The thermal behavior of samples was investigated by thermogravimetric analysis (TGA) with L81A1750 Linseis (Selb, Germany).

**Table 1:** Characterization of PI ww

Parameters	Unit	Concentrations
Chemical oxygen demand-total (COD <sub>total</sub> )	(mg/l)	4000
Chemical oxygen demand-dissolved (COD <sub>dissolved</sub> )	(mg/l)	3200
Biological oxygen demand-5 days (BOD <sub>5</sub> )	(mg/l)	1500
BOD <sub>5</sub> / COD <sub>dissolved</sub>		0.5
Total organic carbons (TOC)	(mg/l)	1800
Dissolved organic carbons (DOC)	(mg/l)	1100
pH		8.3
Salinity as Electrical conductivity (EC)	(mS/cm)	1552
Total alkalinity as CaCO <sub>3</sub>	(mg/l)	750
Total volatile acids (TVA)	(mg/l)	380
Turbidity ( <i>Nephelometric Turbidity unit, NTU</i> )	NTU	7.2
Color	1/m	50
Total suspended solids (TSS)	(mg/l)	250
Volatile suspended solids (VSS)	(mg/l)	187
Total dissolved solids (TDS)	(mg/l)	825
Nitride (NO <sub>2</sub> <sup>-</sup> )	(mg/l)	1.7
Nitrate (NO <sub>3</sub> <sup>-</sup> )	(mg/l)	1.91
Ammonium (NH <sub>4</sub> <sup>+</sup> )	(mg/l)	2.3
Total Nitrogen (Total-N)	(mg/l)	3.2
SO <sub>3</sub> <sup>-2</sup>	(mg/l)	21.4
SO <sub>4</sub> <sup>-2</sup>	(mg/l)	29.3
Chloride (Cl <sup>-</sup> )	(mg/l)	37.4
Bicarbonate (HCO <sub>3</sub> <sup>-</sup> )	(mg/l)	161
Phosphate (PO <sub>4</sub> <sup>-3</sup> )	(mg/l)	16
Total Phosphorus (Total-P)	(mg/l)	40
Total Phenols	(mg/l)	70
Oil & Grease	(mg/l)	220
Cobalt (Co <sup>+3</sup> )	(mg/l)	0.2
Lead (Pb <sup>+2</sup> )	(mg/l)	0.4
Potassium (K <sup>+</sup> )	(mg/l)	17
Iron (Fe <sup>+2</sup> )	(mg/l)	0.42
Chromium (Cr <sup>+2</sup> )	(mg/l)	0.44
Mercury (Hg <sup>+2</sup> )	(mg/l)	0.35
Zinc (Zn <sup>+2</sup> )	(mg/l)	0.11

### 3.3. The Preparation of Carboxymethyl Tragacanth Gum (CMTG)

The CMTG was synthesized according to Abdollahi et al. [80], with slight modifications. 1 g dissolved powdered TG was filled in a mixture of water/ethanol (85 ml/15 ml). Then, 1.2 g NaOH in 10 ml deionized water was added to the reaction mixture. This solution was kept at 50°C for 30 min under a magnetic stirrer (Hedolph, Schwabach, Germany). After, 1.3 g monochloroacetic acid (C<sub>2</sub>H<sub>3</sub>ClO<sub>2</sub>) in 10 ml deionized water was added to the reaction solution, and the final solution was stirred for 4 h at 50°C. After then, cooling, the solution was poured into a double volume of ethanol

or methanol. The resultant CMTG sediment was separated using filter paper and dried at 40°C.

### 3.4. The Synthesis of Fe<sub>2</sub>O<sub>3</sub> NPs

The co-precipitation method was employed for the Fe<sub>2</sub>O<sub>3</sub> NPs synthesis [81]. 0.1 M NaOH solution was added to 100 ml deionized water, and the reaction mixture was stirred magnetically for 15 min under an inert atmosphere [It is an environment where powder bed fusion can take place without the risk of contamination from reactive gases in the air, such as O<sub>2</sub>(g) and CO<sub>2</sub>(g)]. After, a solution of Fe(III) and Fe(II) salts was dropped into the previous

solution, and the final solution was kept under vigorous stirring at 25°C for 70 min. The resulting brown precipitate was separated and washed several times with deionized water and ethanol. After that, the precipitate was dried and the obtained powder was calcined at 300°C for 2 h to gain the Fe<sub>2</sub>O<sub>3</sub> NPs.

### 3.5. The Preparation of CMTG-g-PANI/Fe<sub>2</sub>O<sub>3</sub> BNCs

In a 250 ml round-bottom flask, 0.62 g CMTG was dissolved in 50 ml deionized water. Then, 1.5 ml HCl was added to the solution, and the flask was kept under N<sub>2</sub>(g) at 0–5°C. Subsequently, 10 wt% Fe<sub>2</sub>O<sub>3</sub> NPs (optimum amount) were dispersed in 20 ml deionized water for 30 min using an ultrasonic bath and then added to the above solution. After, within 30 min, 3 g ammonium persulfate [(NH<sub>4</sub>)<sub>2</sub>S<sub>2</sub>O<sub>8</sub>] in 10 ml deionized water was added to the solution. The flask was then placed on a magnetic stirrer for 12 h under the aforementioned conditions after 1.25 ml aniline monomer (C<sub>6</sub>H<sub>5</sub>NH<sub>2</sub>) was added. The NCs was separated by a magnet and rinsed with 10 ml N-methyl pyrrolidone (C<sub>5</sub>H<sub>9</sub>NO), H<sub>2</sub>O and acetone (C<sub>3</sub>H<sub>6</sub>O) before they were dried at 50°C.

### 3.6. Characterization of CMTG-g-PANI/Fe<sub>2</sub>O<sub>3</sub> BNCs

**3.6.1. X-Ray Diffraction (XRD) Analysis:** Powder XRD patterns were recorded on a Shimadzu XRD-7000, Japan diffractometer using Cu K $\alpha$  radiation ( $\lambda = 1.5418 \text{ \AA}$ , 40 kV, 40 mA) at a scanning speed of 1°/min in the 10–80° 2 $\theta$  range. Raman spectrum was collected with a Horiba Jobin Yvon-Labram HR UV-Visible NIR (200–1600 nm) Raman microscope spectrometer, using a laser with the wavelength of 512 nm. The spectrum was collected from 10 scans at a resolution of 2/cm. The zeta potential was measured with a SurPASS Electrokinetic Analyzer (Austria) with a clamping cell at 300 mbar.

**3.6.2. Energy Dispersive X-Ray (EDX) Spectroscopy Analysis:** The elements on the surface of CMTG-g-PANI/Fe<sub>2</sub>O<sub>3</sub> BNCs were analysed using energy dispersive X-ray analysis (EDX) with EDX spectrometry device (TESCAN Co., Model III MIRA).

**3.6.3. Field Emission Scanning Electron Microscopy (FESEM) Analysis:** The morphological features and structure of CMTG-g-PANI/Fe<sub>2</sub>O<sub>3</sub> BNCs was determined by Field Emission Scanning Electron Microscopy (FESEM) (FESEM, Hitachi S-4700).

**3.6.4. Fourier Transform Infrared Spectroscopy (FTIR) Analysis:** The FTIR spectra of experimental samples was recorded using the FT-NIR spectroscope (RAYLEIGH, WQF-510).

**3.6.5. Transmission Electron Microscopy (TEM) Analysis:** The obtained CMTG-g-PANI/Fe<sub>2</sub>O<sub>3</sub> BNCs was collected and harvested by centrifugation (8000 rpm, 5 min), washed twice with deionized water and resuspended in ethanol (C<sub>2</sub>H<sub>6</sub>O) and dripped onto a carbon-coated copper (Cu) TEM grid. Vacuum drying then occurred to the CMTG-g-PANI/Fe<sub>2</sub>O<sub>3</sub> BNCs for 24 h at 25°C. The dry samples on the Cu grid were viewed and examined by TEM Analysis recorded in a JEOL JEM 2100F, Japan under 200 kV accelerating voltage. The size and structure of the CMTG-g-PANI/

Fe<sub>2</sub>O<sub>3</sub> BNCs samples were identified with TEM analysis.

**3.6.6. Value stream mapping (VSM) Analysis:** In order to explain the magnetic property of CMTG-g-PANI/Fe<sub>2</sub>O<sub>3</sub> BNCs, the magnetic hysteresis curve was measured at 25°C. The hysteresis loop exhibits ferromagnetic behavior with saturation magnetization (Ms) of 2.59 emu/g.

**3.6.7. Thermogravimetric Analysis (TGA):** Thermogravimetric analysis (TGA) was done using a Perkin Elmer TGA7 with a temperature range of 25–800°C (with a temperature increase rate of 10°C/min) under constant flow of N<sub>2</sub>(g) and using alumina ceramic crucible. An infrared spectroscope (PERKIN ELMER16F PC FT-IR) equipped with an attenuated total reflectance accessory was used to characterize UiO-66 and UiO-66-Doxycycline complex. Brunauer–Emmet–Teller (BET) measurements were conducted using a Quantachrome Nova touch LX2 model. The samples were purged under vacuum for 4 h at 120°C before initiating the analysis. BET surface area was determined via a multi-point method and the pore parameters were calculated via the Dubinin–Astakhov (DA) method [82]. Dubinin [82], postulated that pore filling is the mechanism of adsorption in micropores. Dubinin [82], developed the theory of volume filling of micropores (TVFM) to explain the pore filling mechanism. Dubinin and Astakhov proposed an equation representing isotherms that obeyed the TVFM. This equation, containing three parameters. is used to characterize the heterogeneity of microporous adsorbents such as activated carbons, zeolites and carbon molecular sieves. The Dubinin-Astakhov (D-A) equation [82], is written as follows (Equation 1):

$$W = W_0 \exp \left[ - \left( \frac{A}{E} \right)^n \right] \quad (1)$$

Where, W: is the amount adsorbed (cc/gm); W<sub>0</sub>: is the volume of micropores (cc/g carbon); E: is the characteristic energy of the adsorption system; n : is the structural heterogeneity parameter, and A : is the adsorption potential.

### 3.7. Adsorption Experiment

CMTG-g-PANI/Fe<sub>2</sub>O<sub>3</sub> BNCs's ability to remove AMX from aqueous solutions was tested in a few different ways. The calibration curve of AMX was prepared by defining the absorbance at 228 nm with a series (1 – 8 mg/l) standard solutions achieved from reducing the stock solution at pH=7.0. After, the AMX initial or equilibrium concentrations were measured with the calibration curve [62].

AMX's initial concentration in an aqueous solution, solution pH, the agitation time, the amount of adsorbent, and other important parameters were all examined for their effects on adsorption capacity. The pH was changed from 4.0 to 9.0 using 0.1 N HCl and 0.1 N NaOH. The optimal adsorption conditions were then investigated using a range of CMTG-g-PANI/Fe<sub>2</sub>O<sub>3</sub> BNCs doses (5–45 mg/l), contact periods (5–40 min.), and initial AMX concentrations (100–500 mg/l). By comparing the outcomes of the experimental data with those predicted by the Langmuir and Freundlich

models, the adsorption isotherms were also explored. To assess the adsorption kinetics, the pseudo-first-order model and the pseudo-second-order model were also applied. The experimental tests were carried out three times, and an average of the results was provided. A UV-visible spectrometer (Cary 5000 UV-Vis Spectrophotometer from Varian, Siemens, Germany) was used to assess the AMX concentration. AMX's capacity and adsorption efficiency onto CMTG-g-PANI/Fe<sub>2</sub>O<sub>3</sub> BNCs were calculated using **Equation (2)** and **Equation (3)**, respectively [42].

$$R\% = \left[ \frac{(C_i - C_e)}{C_i} \right] \times 100 \quad (2)$$

$$Q_e = \left[ \frac{(C_i - C_e)}{m} \right] \times V \quad (3)$$

Where, C<sub>i</sub> : is the AMX initial concentration in the solutions (mg/l); C<sub>e</sub> : is the equilibrium concentration in the solutions (mg/l); m : is the weight of CMTG-g-PANI/Fe<sub>2</sub>O<sub>3</sub> BNCs (g); V : is the solution volume (l), respectively.

### 3.8. The Study of Isotherm

Langmuir and Freundlich's isotherm models are used to evaluate the maximum adsorption capacity isotherm and the equilibrium adsorption isotherm. The Langmuir isotherm model measured the single-layer adsorption of contaminants onto the adsorbent surface, whereas the Freundlich isotherm model measured the multi-layer adsorption of pollutants on the adsorbent surface. The mathematical expression of the Langmuir's isotherm model (Equation 4) and the Freundlich's isotherm model (Equation 5) are as follows [62, 83]:

$$\frac{C_e}{Q_e} = \frac{1}{K_L Q_{max}} + \frac{1}{Q_{max}} C_e \quad (4)$$

$$\ln Q_e = \ln K_F + \frac{1}{n} \ln C_e \quad (5)$$

where, C<sub>e</sub> : is the equilibrium concentration (mg/l), Q<sub>e</sub> : is the equilibrium adsorption capacity (mg/g); Q<sub>max</sub> : is the maximum adsorption capacity (mg/g); K<sub>L</sub> : is the Langmuir constant calculated from the plot between C<sub>e</sub>/Q<sub>e</sub> and C<sub>e</sub> (l/mg); K<sub>F</sub> : is the Freundlich constant calculated from the plot between LnQ<sub>e</sub> and LnC<sub>e</sub> (l/mg); n : is a parameter to define the adsorption process favorability, respectively. If n > 1, high concentrations of AMX adsorption on the bioadsorbent are expected.

### 3.9. The Study of Kinetic

The famous kinetics models were used for studying the effect of time on the adsorption process. The mathematical expression of the pseudo-first-order model (Equation 6) and the pseudo-second-order model (Equation 7) are shown in following [62, 83]:

$$\ln(Q_e - Q_t) = \ln Q_e - k_1 t \quad (6)$$

$$\frac{t}{Q_t} = \frac{1}{k_2 Q_e^2} + \frac{1}{Q_e} t \quad (7)$$

where Q<sub>t</sub> : is the adsorption capacity at time t (mg/g); Q<sub>e</sub> : is the adsorption capacity at equilibrium (mg/g); k<sub>1</sub> : is the rate constant of pseudo-first-order (1/min); k<sub>2</sub> : is the rate constants of the pseudo-second-order (g/mg·min), respectively.

### 3.10. The Study of Desorption and Reusability

To examine the desorption and reusability of CMTG-g-PANI/Fe<sub>2</sub>O<sub>3</sub> BNCs, AMX adsorbed onto CMTG-g-PANI/Fe<sub>2</sub>O<sub>3</sub> BNCs was floated in ethanol and stirred at 25°C for 1 h. After, the CMTG-g-PANI/Fe<sub>2</sub>O<sub>3</sub> BNCs was separated by a magnet. The quantity of released AMX in the elution medium was measured then employing a UV-visible spectrophotometer (Cary 5000 UV-Vis Spectrophotometer from Varian, Siemens, Germany). The desorption percentage was shown following in Equation (8).

$$\%D = \frac{A}{B} \times 100 \quad (8)$$

Where, A: is the AMX desorbed in the medium (mg); B : is the AMX adsorbed on the CMTG-g-PANI/Fe<sub>2</sub>O<sub>3</sub> BNCs (mg).

### 3.11. Analytical Procedures

COD<sub>total</sub>, COD<sub>dissolved</sub>, Total-P, PO<sub>4</sub><sup>3-</sup>-P, Total-N, NH<sub>4</sub><sup>+</sup>-N, NO<sub>3</sub><sup>-</sup>-N, NO<sub>2</sub><sup>-</sup>-N, BOD<sub>5</sub>, pH, T(°C), TSS, TVSS, TOC, Oil, Cl<sup>-</sup>, total phenol, TVA, DOC, total alkalinity, turbidity, TDS, color, SO<sub>3</sub><sup>2-</sup>, SO<sub>4</sub><sup>2-</sup>, HCO<sub>3</sub><sup>-</sup>, salinity, Co<sup>+3</sup>, Pb<sup>+2</sup>, K<sup>+</sup>, Fe<sup>+2</sup>, Cr<sup>+2</sup>, Hg<sup>+2</sup> and Zn<sup>+2</sup> were measured according to the Standard Methods (2017) 5220B, 5220D, 4500-P, 4500-PO<sub>4</sub><sup>3-</sup>, 4500-N, 4500-NH<sub>4</sub><sup>+</sup>, 4500-NO<sub>3</sub><sup>-</sup>, 4500-NO<sub>2</sub><sup>-</sup>, 5210B, 4500-H<sup>+</sup>, 2320, 2540D, 2540E, 5310, 5520, 4500-Cl<sup>-</sup>, 5530, 5560B, 5310B, 2320, 2130, 2540E, 2120, 4500-SO<sub>3</sub><sup>2-</sup>, 4500-SO<sub>4</sub><sup>2-</sup>, 5320, 2520, 3500-Co<sup>+3</sup>, 3500-Pb<sup>+2</sup>, 3500-K<sup>+</sup>, 3500-Fe<sup>+2</sup>, 3500-Cr<sup>+2</sup>, 3500-Hg<sup>+2</sup>, 3500-Zn<sup>+2</sup>, respectively [84].

Total-N, NH<sub>4</sub><sup>+</sup>-N, NO<sub>3</sub><sup>-</sup>-N, NO<sub>2</sub><sup>-</sup>-N, Total-P, PO<sub>4</sub><sup>3-</sup>-P, total phenol, Co<sup>+3</sup>, Pb<sup>+2</sup>, K<sup>+</sup>, Fe<sup>+2</sup>, Cr<sup>+2</sup>, Hg<sup>+2</sup>, Zn<sup>+2</sup>, SO<sub>3</sub><sup>2-</sup>, and SO<sub>4</sub><sup>2-</sup> were measured with cell test spectroquant kits (Merck, Germany) at a spectroquant NOVA 60 (Merck, Germany) spectrophotometer (2003).

The measurement of color was carried out following the methods described by Olthof and Eckenfelder [85], and Eckenfelder [86]. According these methods, the color content was determined by measuring the absorbance at three wavelengths (445 nm, 540 nm and 660 nm), and taking the sum of the absorbances at these wavelengths. In order to identify the color in 25 ml PI ww was acidified at pH=2.0 with a few drops of 6 N HCl and extracted three times with 25 ml of ethyl acetate. The pooled organic phases were dehydrated on sodium sulphate, filtered and dried under vacuum. The residue was silylated with bis(trimethylsilyl)trifluoroacetamide (BSTFA) in dimethylformamide and analyzed by gas chromatography–mass spectrometry (GC-MS) and gas chromatograph (GC) (Agilent Technology model 6890N) equipped with a mass selective detector (Agilent 5973 inert MSD). Mass spectra were recorded using a VGTS 250 spectrometer equipped with a capillary SE 52 column (HP5-MS 30 m, 0.25 mm ID, 0.25 μm) at 220°C with an isothermal program for 10 min. The initial oven temperature was kept at 50°C for 1 min, then raised to 220°C at 25°C/min and from 200 to 300°C at 8°C/min, and was then maintained for 5.5 min. High purity He (g) was used as the carrier gas at constant flow mode (1.5 ml/min, 45 cm/s linear velocity).

The total phenol was monitored as follows: 40 ml of PI ww was

acidified to pH=2.0 by the addition of concentrated HCl. Total phenol was then extracted with ethyl acetate. The organic phase was concentrated at 40°C to about 1 ml and silylized by the addition of N,O-bis(trimethylsilyl) acetamide (BSA). The resulting trimethylsilyl derivatives were analysed by GC-MS (Hewlett-Packard 6980/HP5973MSD).

Methyl tertiary butyl ether (MTBE) was used to extract oil from the water and NPs. GC-MS analysis was performed on an Agilent gas chromatography (GC) system. Oil concentration was measured using a UV-vis fluorescence spectrophotometer (Cary 5000 UV-Vis Spectrophotometer from Varian, Siemens, Germany) and a GC-MS (Hewlett-Packard 6980/HP5973MSD). UV-vis absorbance was measured on this UV-vis fluorescence spectrophotometer and oil concentration was calculated using a calibration plot which was obtained with known oil concentration samples.

### 3.12. Statistical Analysis

ANOVA analysis of variance between experimental data was performed to detect *F* and *P* values. The ANOVA test was used to test the differences between dependent and independent groups, [87]. (Zar, 1984). Comparison between the actual variation of the experimental data averages and standard deviation is expressed in terms of *F* ratio. *F* is equal (found variation of the date averages/expected variation of the date averages). *P* reports the significance level, and d.f indicates the number of degrees of freedom. Regression analysis was applied to the experimental data in order to determine the regression coefficient  $R^2$ , [88]. The aforementioned test was performed using Microsoft Excel Program.

All experiments were carried out three times and the results are given as the means of triplicate samplings. The data relevant to the individual pollutant parameters are given as the mean with standard deviation (SD) values.

## 4. Results and Discussions

### 4.1. The Characteristics of CMTG-g-PANI/Fe<sub>2</sub>O<sub>3</sub> BNCs

**4.1.1. The Results of XRD Analysis:** The results of XRD analysis was observed to CMTG-g-PANI/Fe<sub>2</sub>O<sub>3</sub> BNCs in the removal of AMX in PI ww with adsorption process (Figure 1). The characterization peaks were found at  $2\theta$  values of 22.18° and corresponding to the (110), respectively (Figure 1a). The characterization peaks were measured at  $2\theta$  values of 33.41°, 36.10°, 50.28°, 55.71°, 62.38° and 64.60°, respectively, and corresponding to the (003), (112), (200), (120), (222) and (221), respectively (Figure 1b). The characterization peaks were observed at  $2\theta$  values of 22.19°, 24.03° and 33.11°, respectively, and corresponding to the (101), (114) and (120), respectively (Figure 1c). The characterization peaks were measured at  $2\theta$  values of 34.12°, 36.81°, 49.76° and 54.63°, respectively, and corresponding to the (112), (042), (211) and (132), respectively (Figure 1d).

**4.1.2. The Results of EDX Analysis:** The EDX analysis of CMTG-g-PANI/Fe<sub>2</sub>O<sub>3</sub> BNCs was also performed to investigate in the removal of AMX in PI ww with adsorption process (Figure 2). The elemental percentages of CMTG-g-PANI/Fe<sub>2</sub>O<sub>3</sub> BNCs were obtained at 41.50w%C, 27.80w%O, 12.66w%N, 7.56w%Fe, 5.37w%Cl and 5.11w%Na, respectively (Figure 2).

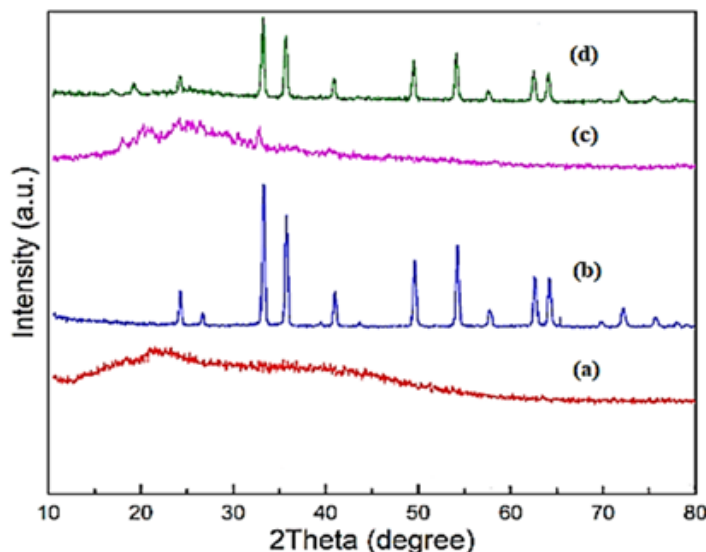


**Figure 1:** XRD spectra of (a) CMTG NPs, (b) Fe<sub>2</sub>O<sub>3</sub> NPs, (c) CMTG-g-PANI NCs and (d) CMTG-g-PANI/Fe<sub>2</sub>O<sub>3</sub> BNCs in the removal of AMX in PI ww with adsorption process.

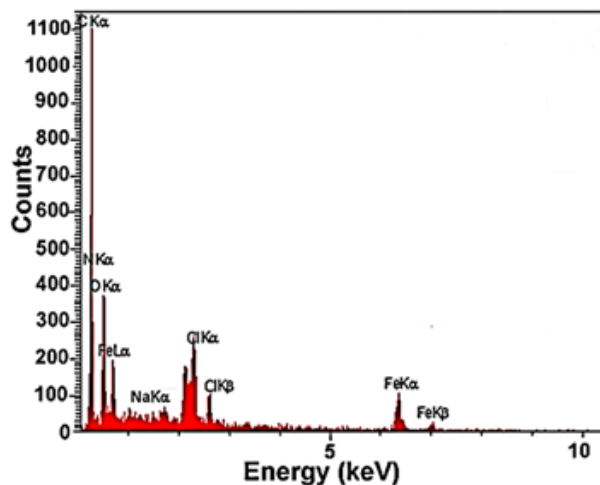


**Figure 2:** EDX spectrum of CMTG-g-PANI/Fe<sub>2</sub>O<sub>3</sub> BNCs in the removal of AMX in PI ww with adsorption process.

**4.1.3. The Results of FESEM Analysis:** The morphological features of CMTG, PANI, Fe<sub>2</sub>O<sub>3</sub> NPs and CMTG-g-PANI/Fe<sub>2</sub>O<sub>3</sub> BNCs were characterized through FE-SEM images (Figure 3). The FESEM images of CMTG (Figure 3a), PANI (Figure 3b), Fe<sub>2</sub>O<sub>3</sub> NPs (Figure 3c) and CMTG-g-PANI/Fe<sub>2</sub>O<sub>3</sub> BNCs (Figure 3d) were observed in the removal of AMX in PI ww with adsorption process. The FESEM images size is 200 nm (Figure 3).

**4.1.4. The Results of FTIR Analysis:**

The FTIR spectrum of CMTG NPs, Fe<sub>2</sub>O<sub>3</sub> NPs, CMTG-g-PANI NCs and CMTG-g-PANI/Fe<sub>2</sub>O<sub>3</sub> BNCs were obtained in the removal of AMX in PI ww with adsorption process (Figure 4).

The main peaks of FTIR spectrum CMTG NPs for AMX removal in PI ww with adsorption process was observed at 1650 1/cm and 1430 1/cm wavenumber, respectively (Figure 4a). The main peaks of FTIR spectrum Fe<sub>2</sub>O<sub>3</sub> NPs for AMX removal in PI ww with adsorption process was obtained at 1600 1/cm and 650 1/cm wavenumber, respectively (Figure 4b). The main peaks of FTIR spectrum CMTG-g-PANI NCs for AMX removal in PI ww with adsorption process was measured at 1635 1/cm, 1438 1/cm and 1112 1/cm wavenumber, respectively (Figure 4c). The main peaks of FTIR spectrum CMTG NPs for AMX removal in PI ww with adsorption process was found at 1617 1/cm, 1395 1/cm and 1100 1/cm wavenumber, respectively (Figure 4d).

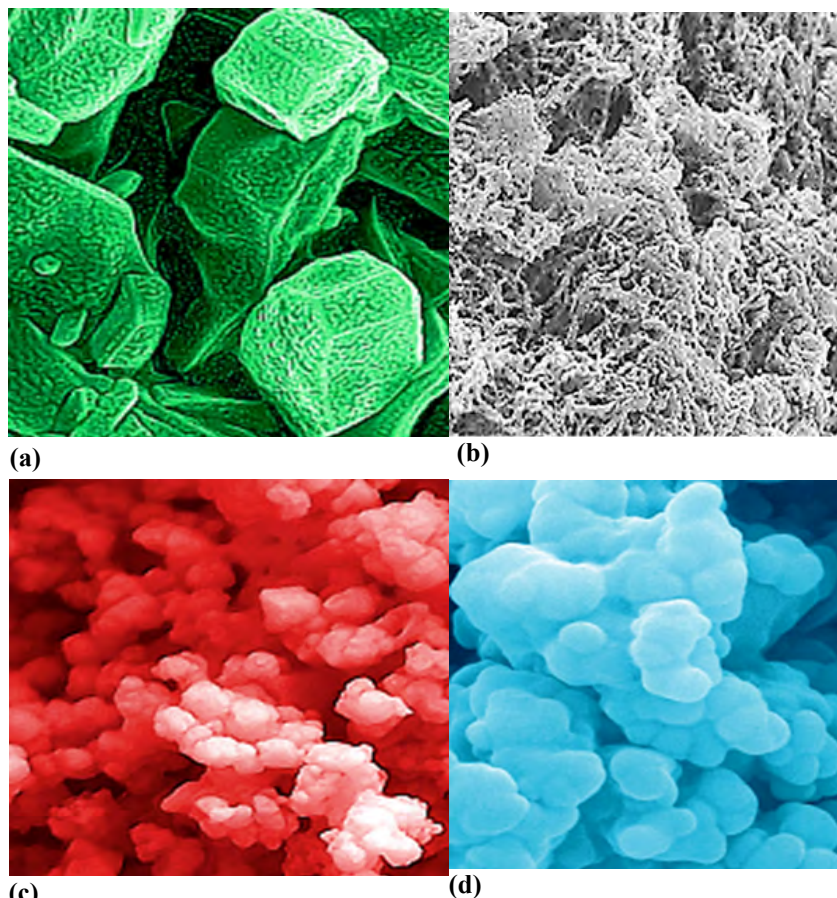


**Figure 3:** FESEM images of (a) CMTG, (b) PANI (c) Fe<sub>2</sub>O<sub>3</sub> NPs and (d) CMTG-g-PANI/Fe<sub>2</sub>O<sub>3</sub> BNCs in the removal of AMX in PI ww with adsorption process (FESEM images size: 200 nm).

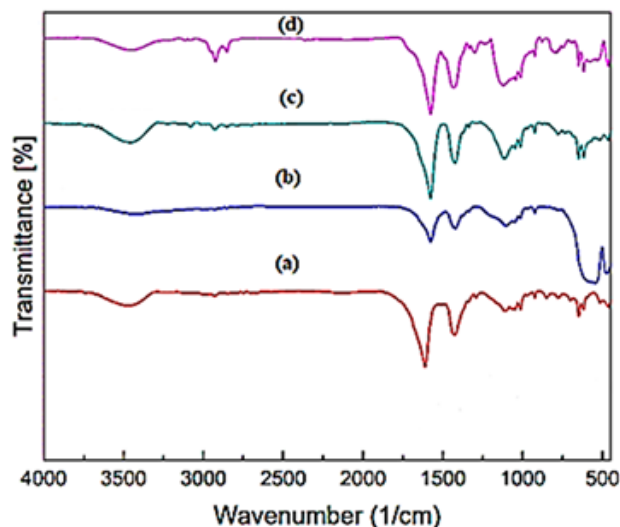


**Figure 4:** FTIR spectrum of (a) CMTG NPs, (b)  $\text{Fe}_2\text{O}_3$  NPs, (c) CMTG-g-PANI NCs and (d) CMTG-g-PANI/ $\text{Fe}_2\text{O}_3$  BNCs in the removal of AMX in PI ww with adsorption process.

#### 4.1.5. The Results of TEM Analysis:

The TEM images of CMTG-g-PANI/ $\text{Fe}_2\text{O}_3$  BNCs was obtained in the removal of AMX in PI ww with adsorption process (Figure 5).

#### 4.1.6. The Results of VSM and TGA Analysis

The VSM curve of CMTG-g-PANI/ $\text{Fe}_2\text{O}_3$  BNCs (Figure 6a) and the TGA thermogram of CMTG (blue line), CMTG-g-PANI (red dashed line) and CMTG-g-PANI/ $\text{Fe}_2\text{O}_3$  BNCs (green dotted line), respectively, (Figure 6b) in the removal of AMX in PI ww with adsorption process.

VSM analysis was employed to evaluate of magnetic properties of CMTG-g-PANI/ $\text{Fe}_2\text{O}_3$  BNCs as shown in Figure 6a. The magnetization saturation ( $M_s$ ) value of and CMTG-g-PANI/ $\text{Fe}_2\text{O}_3$  BNCs was 23 emu/g and showed superparamagnetic properties (Figure 6a).

TG analysis was applied to study the thermal stability of prepared materials as seen in Figure 6b. The char yield of TG at 800°C was 25wt%. Four mass losses at 30–150°C, 150–300°C, 300–550°C

and 550–780°C were measured in the TGA thermogram of CMTG. The first (10wt%) and second (32wt%) mass losses were related to the moisture evaporation and combination of the saccharide ring degradation, the C–O–C breaking, and  $\text{CO}_2(\text{g})$  elimination from CMTG, respectively [89, 90]. The two latter mass losses were attributed to the CMTG backbone breaking [90]. The char yield of CMTG at 800°C was 33wt%. In the TGA thermogram of CMTG-g-PANI, four mass losses were obtained. The first mass loss (10wt%) at 5–200°C was caused by the evaporation of  $\text{H}_2\text{O}$  and solvent entrapment in the co-polymer chains [91]. The second mass loss (25wt%) at 200–300°C probably corresponded to the loss of hydrochloric acid (HCl), saccharide ring, and  $\text{CO}_2(\text{g})$  elimination from CMTG-g-PANI NCs. The third mass loss (10wt%) at 300–500°C and the fourth mass loss (20wt%) at 500–750°C was ascribed to the breakdown of sugar units in CMTG structure and PANI, respectively. The char yield of CMTG-g-PANI at 800°C was 34wt%. Compared with CMTG-g-PANI NCs, the TGA thermogram of CMTG-g-PANI/ $\text{Fe}_2\text{O}_3$  BNCs was shown good thermal stability owing to the existence of  $\text{Fe}_2\text{O}_3$  NPs in CMTG-g-PANI NCs matrix.

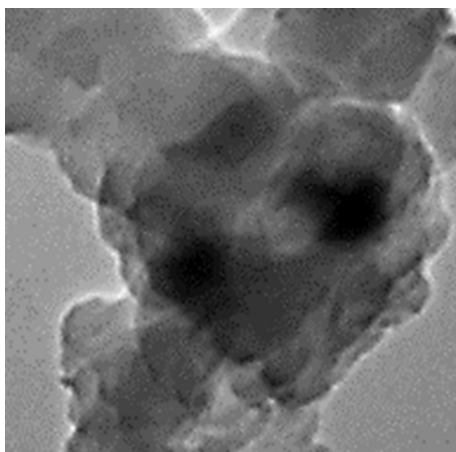


**Figure 5:** TEM images of CMTG-g-PANI/ $\text{Fe}_2\text{O}_3$  BNCs was obtained in the removal of AMX in PI ww with adsorption process.

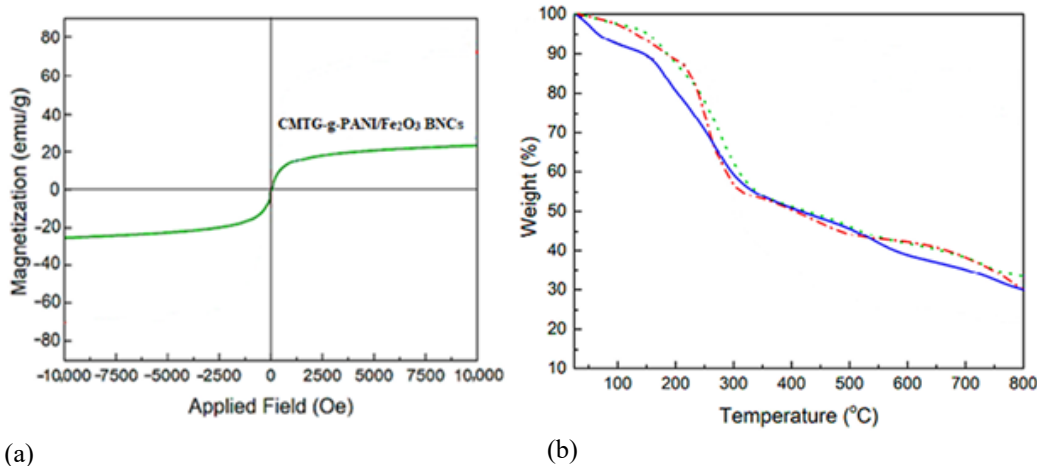


**Figure 6:** (a) The VSM curve of CMTG-g-PANI/Fe<sub>2</sub>O<sub>3</sub> BNCs and (b) the TGA thermogram of CMTG (blue line), CMTG-g-PANI (red dashed line) and CMTG-g-PANI/Fe<sub>2</sub>O<sub>3</sub> BNCs (green dotted line), respectively, in the removal of AMX in PI ww with adsorption process.

### 4.2. Adsorption Isotherm Models

Isotherm study was used to find the interaction between AMX and CMT-g-PANI/Fe<sub>2</sub>O<sub>3</sub> BNCs. It is well known that Langmuir and Freundlich’s isotherm models are used to evaluate the maximum adsorption capacity and equilibrium adsorption isotherms. The obtained parameters of isotherm models are shown in Table 2. Consistent with obtained the isotherm models correlation coefficients (R<sup>2</sup>), the Freundlich isotherm model was found to be more reliable with the experimental data than the Langmuir isotherm model. This result shows that AMX adsorbed over CMTG-g-PANI/Fe<sub>2</sub>O<sub>3</sub> BNCs bioadsorbent surface as a multilayer. Therefore, the obtained “n” in the Freundlich isotherm model is an important parameter to define the adsorption process favorability. The value of n > 1 in Table 2 shows that AMX adsorbed over CMTG-g-PANI/Fe<sub>2</sub>O<sub>3</sub> BNCs bioadsorbent surface is desirable at high concentrations. The comparison of Q<sub>max</sub> for AMX to other adsorbents reported in recent years showed that CMTG-g-PANI/Fe<sub>2</sub>O<sub>3</sub> BNCs biosorbent has Q<sub>max</sub> = 983.11 mg/g maximum adsorption capacity. This could be related to the presence of Fe<sub>2</sub>O<sub>3</sub> NPs and numerous active sites (such as, hydroxyl, carboxylate, and amine groups in the NCs), which can effectively interact with AMX (via electrostatic interaction and hydrogen bonding), led to eliminating AMX.

**Table 2.** The adsorption isotherm model parameters for AMX adsorption onto CMTG-g-PANI/Fe<sub>2</sub>O<sub>3</sub> BNCs

Parameters	Adsorption Isotherm Models	
	Langmuir	Freundlich
K <sub>p</sub>		89.9721
n		1.99
R <sup>2</sup>	0.9106	0.9985
Q <sub>max</sub>	983.11	
K <sub>L</sub>	0.0567	

### 4.3. Adsorption Kinetic Models

The pseudo-first-order kinetic model and the pseudo-second-order kinetic model were used to explore and evaluate the adsorption pathways, equilibrium time and adsorption rate limiting phase of AMX adsorbed on CMT-g-PANI/Fe<sub>2</sub>O<sub>3</sub> BNCs adsorbent. However, kinetic models are employed to define the adsorption process mechanism, for instance, surface adsorption and chemical adsorption. The pseudo-first-order kinetic model is based on the adsorbent capacity and employed once adsorption happens via diffusion in a border layer, whereas the pseudo-second-order kinetic model expresses that the chemical adsorption procedure is the main controlling procedure. The parameters calculated from the pseudo-first-order kinetic model and the pseudo-second-order adsorption kinetic model are given in Table 3. According to R<sup>2</sup>, the difference between the estimated Q<sub>e</sub> and observed Q<sub>e</sub> values, the pseudo-second-order kinetic model is more appropriate for considering the AMX adsorption kinetics on CMTG-g-PANI/Fe<sub>2</sub>O<sub>3</sub> BNCs. In conclusion, chemical adsorption is the main mechanism in AMX adsorption on the adsorbent and it displays that, in addition to AMX molecules, CMTG-g-PANI/Fe<sub>2</sub>O<sub>3</sub> BNCs bioadsorbent is involved in the adsorption procedure.

**Table 3.** The adsorption kinetic models parameters for AMX adsorption on CMTG-g-PANI/Fe<sub>2</sub>O<sub>3</sub> BNCs.

Parameters	Adsorption Kinetic Models	
	Pseudo-first-order	Pseudo-second-order
k <sub>1</sub>	0.0739	
k <sub>2</sub>		0.000001
Q <sub>e</sub> calculated	38.564	
Q <sub>e</sub> experimental	791.42	791.56
Q <sub>e</sub>		834.12
R <sup>2</sup>	0.9867	0.9929

#### 4.4. The Desorption and Reusability of CMTG-g-PANI/Fe<sub>2</sub>O<sub>3</sub> BNCs for AMX Adsorption in Surface Water

The reusability of adsorbent is a significant factor to create the adsorption procedure economically. The reusability of adsorbent can be effective for its use in numerous consecutive cycles without considerable performance debility. The AMX desorption and reusability of CMT-g-PANI/Fe<sub>2</sub>O<sub>3</sub> BNCs bioadsorbent were evaluated in three consecutive cycles, and an ethanolic solution was investigated. In this regard, AMX adsorbed onto CMTG-g-PANI/Fe<sub>2</sub>O<sub>3</sub> BNCs was performed in optimal conditions and was immersed into 10 ml ethanol under stirring at 25°C for 60 min to

desorb AMX. After, CMTG-g-PANI/Fe<sub>2</sub>O<sub>3</sub> BNCs was collected by a magnet, washed with deionized water, and then dried for successive adsorption/desorption processes. Then, the released AMX amount in the elution medium was measured using the UV-vis fluorescence spectrophotometer. Figure 7 shows that the adsorption percentage decreased from 98.59 % to 94.03%, and the desorption percentage decreased from 94.41% to 92.001% after three consecutive cycles, these results show that the CMT-g-PANI/Fe<sub>2</sub>O<sub>3</sub> BNCs could continue to remove amoxicillin after three consecutive cycles of adsorption/desorption process without considerably losing adsorption capacity.

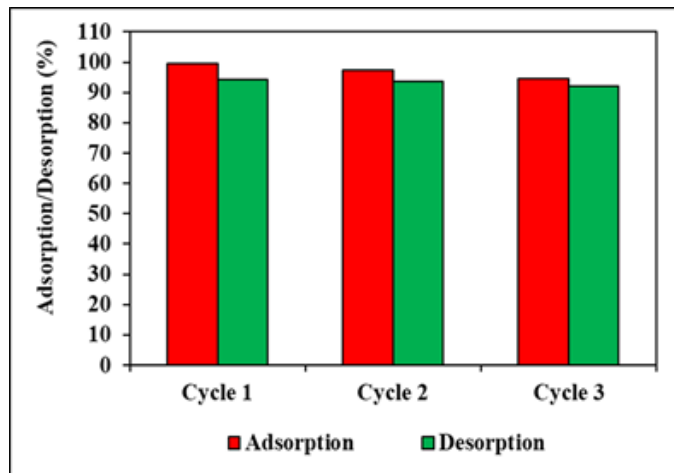


Figure 7. The desorption and reusability of CMTG-g-PANI/Fe<sub>2</sub>O<sub>3</sub> BNCs bioadsorbent for AMX adsorption in surface water.

#### 4.5. The Adsorption Mechanism of AMX

The pollutant adsorption mechanism by the bioadsorbent depends on the functional groups and morphology of bioadsorbent, which can be created a synergistic effect in increasing the pollutant adsorption by the bioadsorbent. Considering that the CMTG-g-

PANI/Fe<sub>2</sub>O<sub>3</sub> BNCs bioadsorbent has amine, carboxylate, and hydroxyl functional groups, it can create intermolecular interactions (hydrogen bonding, electrostatic and  $\pi$ - $\pi$  interactions) with the AMX, and cause its efficient adsorption on the CMTG-g-PANI/Fe<sub>2</sub>O<sub>3</sub> BNCs bioadsorbent as seen in Figure 8.

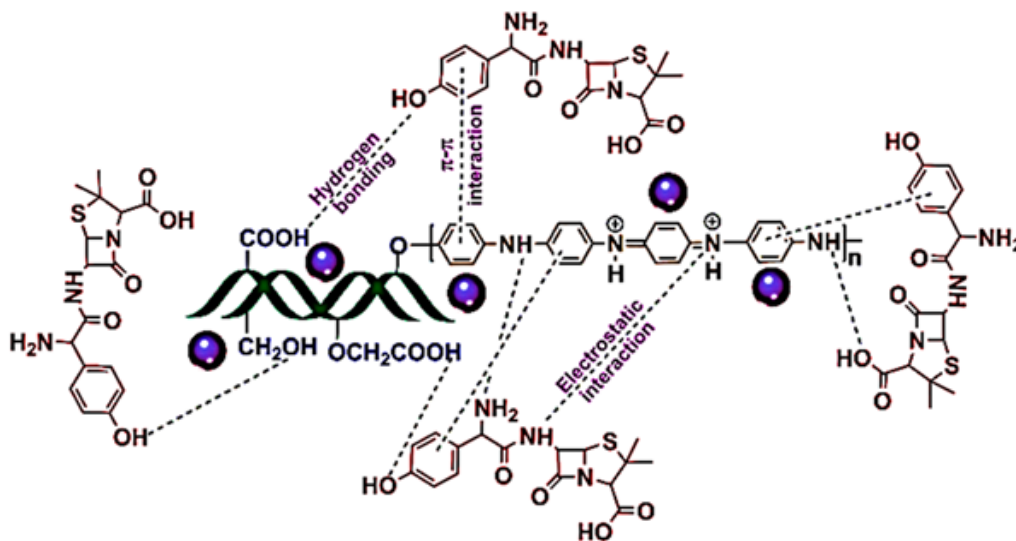


Figure 8. The adsorption mechanism of AMX in surface water using CMTG-g-PANI/Fe<sub>2</sub>O<sub>3</sub> BNCs.

#### 4.6. Effect of Increasing pH values for AMX Removal in PI ww with Adsorption Process

Increasing pH values (4.0, 5.0, 7.0 and 9.0) was examined during adsorption process in PI ww for AMX removal in surface water at 25°C, respectively (Figure 9). 65.18%, 70.29% and 50.84% AMX removals were measured at pH=4.0, pH=5.0 and pH=9.0, respectively, at 25°C (Figure 9). The maximum 99.36% AMX removal efficiency was obtained during adsorption process in PI ww at pH=7.0 and at 25°C (Figure 9).

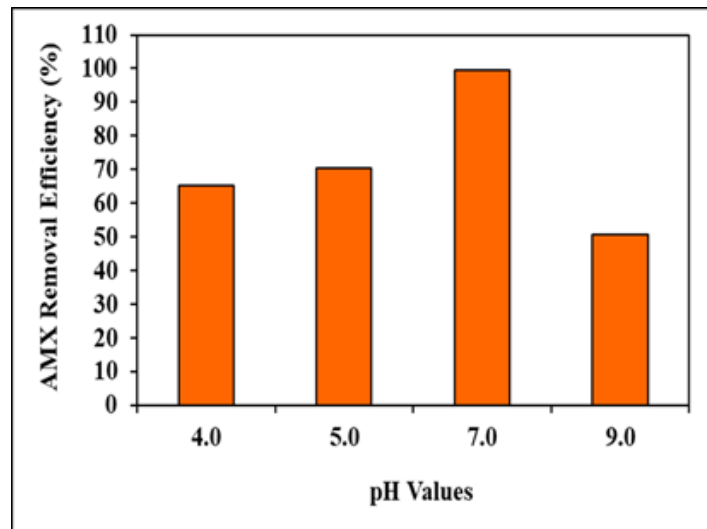


Figure 9: Effect of increasing pH values for AMX removal in PI ww during adsorption process at 25°C.

#### 4.7. Effect of Increasing Adsorption Time for AMX Removal in PI ww with Adsorption Process

Increasing adsorption times (5 min, 10 min, 20 min and 40 min) was operated during adsorption process in PI ww for AMX removal in surface water, at pH=7.0 and at 25°C, respectively (Figure 10). 66.25%, 81.11% and 57.82% AMX removals were found after 5 min, 10 min and 40 min, respectively, at pH=7.0 and at 25°C (Figure 10). The maximum 99.07% AMX removal efficiency was observed during adsorption process in PI ww after 20 min adsorption time, at pH=7.0 and at 25°C, respectively (Figure 10).

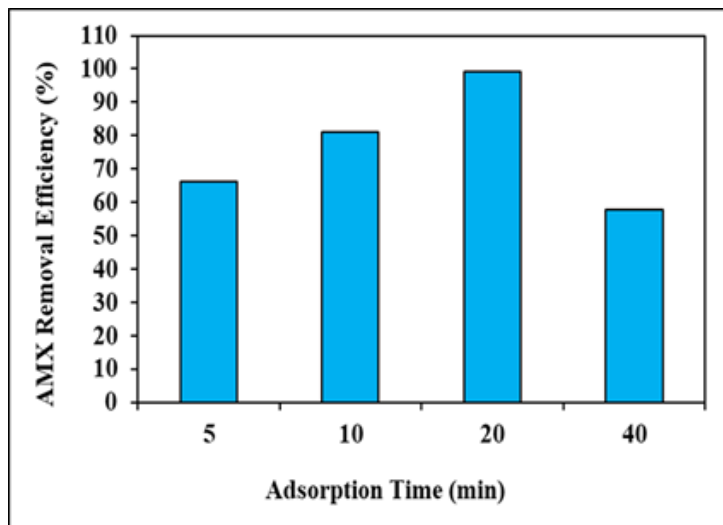
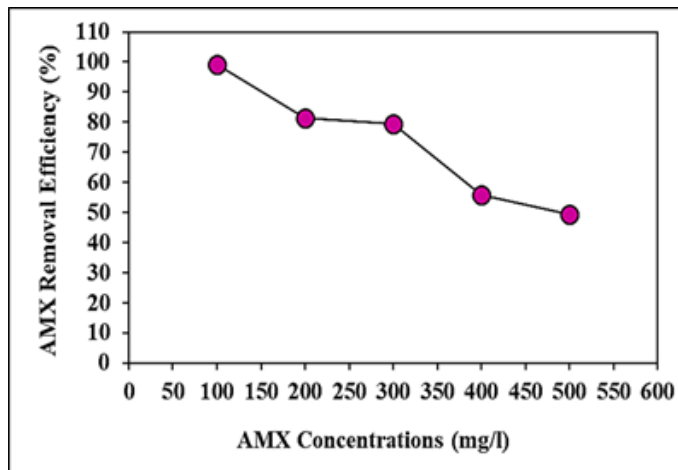


Figure 10: Effect of increasing adsorption times for AMX removal in PI ww during adsorption process, at pH=7.0 and at 25°C.

#### 4.8. Effect of Increasing AMX Concentrations for AMX Removal in PI ww during Adsorption Process

Increasing AMX concentrations (100 mg/l, 200 mg/l, 300 mg/l, 400 mg/l and 500 mg/l) were operated after 120 min adsorption time, at pH=7.0 and at 25°C, respectively (Figure 11). 81.34%, 79.40%, 55.73% and 49.26% AMX removal efficiencies were ob-

tained to 200 mg/l, 300 mg/l, 400 mg/l and 500 mg/l AMX concentrations, after 20 min adsorption time, at pH=7.0 and at 25°C, respectively (Figure 11). The maximum 99.23% AMX removals efficiency was found with adsorption process in PI ww, at 100 mg/l AMX, after 20 min adsorption time, at pH=7.0 and at 25°C, respectively (Figure 11).



**Figure 11:** Effect of increasing AMX concentrations for AMX removal in PI ww during adsorption process, after 20 min adsorption time, at pH=7.0 and at 25°C, respectively.

**4.9 Effect of Increasing CMTG-g-PANI/Fe<sub>2</sub>O<sub>3</sub> BNCs Concentrations for AMX Removals in PI ww during Adsorption Process**

Increasing CMTG-g-PANI/Fe<sub>2</sub>O<sub>3</sub> BNCs concentrations (5 mg/l, 15 mg/l, 30 mg/l and 45 mg/l) were operated at 100 mg/l AMX after 20 min adsorption time, at pH=7.0 and at 25°C, respectively (Figure 12). 77.41%, 64.08% and 45.79% AMX removal efficiencies were obtained to 15 mg/l, 30 mg/l and 45 mg/l CMTG-g-PANI/Fe<sub>2</sub>O<sub>3</sub> BNCs concentrations, respectively, at 100 mg/l AMX after 20 min adsorption time, at pH=7.0 and at 25°C, respectively (Figure 12). The maximum 99.20% AMX removal efficiency was measured to 5 mg/l CMTG-g-PANI/Fe<sub>2</sub>O<sub>3</sub> BNCs with adsorption process in PI ww, at 100 mg/l AMX after 20 min adsorption time, at pH=7.0 and at 25°C, respectively (Figure 12).

**4.10. Effect of Different Recycle Times for AMX Removals in PI ww during Adsorption Process**

Different recycle times (between 1. and 20.) were operated for AMX removals in PI ww during adsorption process, at 100 mg/l AMX after 20 min adsorption time, at pH=7.0 and at 25°C, respectively (Figure 13). 98%, 97%, 95%, 94%, 92%, 90%, 88%, 86%, 84%, 83%, 82%, 81%, 80%, 78%, 75%, 72%, 70% and 61% AMX recovery yields were measured after 3., 4., 5., 6., 7., 8., 9., 10., 11., 12., 13., 14., 15., 16., 17., 18., 19., and 20. recycle times, respectively, at 100 mg/l AMX after 20 min adsorption time, at pH=7.0 and at 25°C, respectively (Figure 13). The maximum 99% and 99% AMX recovery efficiencies were measured in PI ww during adsorption process, after 1. recycle time and 2. recycle time, respectively, at 100 mg/l AMX after 20 min adsorption time, at pH=7.0 and at 25°C, respectively (Figure 13).

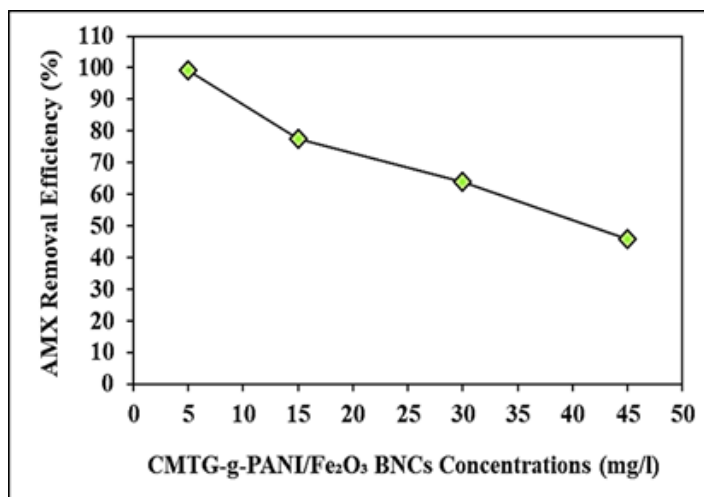


**Figure 12:** Effect of increasing CMTG-g-PANI/Fe<sub>2</sub>O<sub>3</sub> BNCs concentrations for AMX removal in PI ww during adsorption process, at 100 mg/l AMX after 20 min adsorption time, at pH=7.0 and at 25°C, respectively.

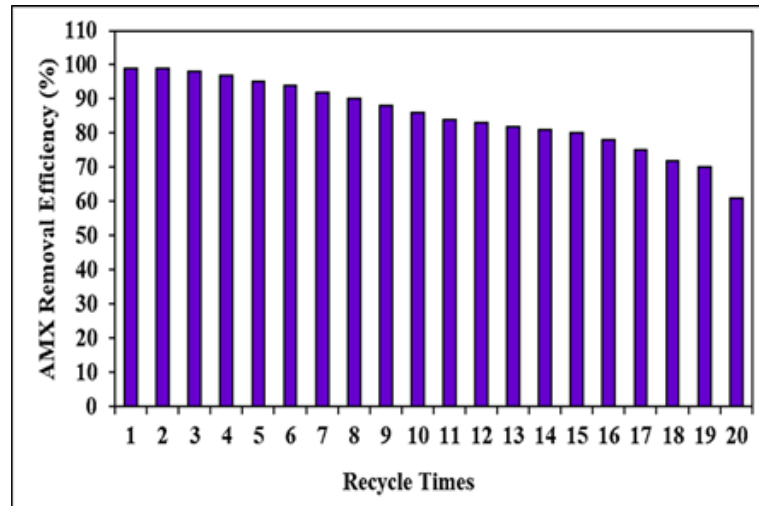


**Figure 13:** Effect of recycle times for AMX removal in PI ww during adsorption process, at 100 mg/l AMX, 5 mg/l CMTG-g-PANI/Fe<sub>2</sub>O<sub>3</sub> BNCs after 20 min adsorption time, at pH=7.0 and at 25°C, respectively.

## 5. Conclusions

The treatment of AMX antibiotic from the surface water using CMTG-g-PANI/Fe<sub>2</sub>O<sub>3</sub> BNCs as a bioadsorbent was examined with adsorption process from PI ww plant, İzmir, Turkey. The maximum 99.36% AMX removal efficiency was obtained during adsorption process in PI ww at pH=7.0 and at 25°C. The maximum 99.07% AMX removal efficiency was observed during adsorption process in PI ww after 20 min adsorption time, at pH=7.0 and at 25°C, respectively. The maximum 99.23% AMX removals efficiency was found with adsorption process in PI ww, at 100 mg/l AMX, after 20 min adsorption time, at pH=7.0 and at 25°C, respectively. The maximum 99.20% AMX removal efficiency was measured to 5 mg/l CMTG-g-PANI/Fe<sub>2</sub>O<sub>3</sub> BNCs with adsorption process in PI ww, at 100 mg/l AMX after 20 min adsorption time, at pH=7.0 and at 25°C, respectively. The maximum 99% and 99% AMX recovery efficiencies were measured in PI ww during adsorption process, after 1. recycle time and 2. recycle time, respectively, at 100 mg/l AMX after 20 min adsorption time, at pH=7.0 and at 25°C, respectively.

A granular structure with good thermal stability (34wt% char yield), 8.1143 m<sup>2</sup>/g specific surface area and 23 emu/g magnetization saturation were measured for CMTG-g-PANI/Fe<sub>2</sub>O<sub>3</sub> BNCs. 983.11 mg/g maximum adsorption capacity was observed at pH=7.0, at 20 min adsorption mixing time, at 5 mg/l CMTG-g-PANI/Fe<sub>2</sub>O<sub>3</sub> BNCs, at 500 mg/l initial AMX concentration, respectively. The Freundlich isotherm model and the pseudo-second-order kinetic models are much more suitable with the experimental data for AMX removal in PI ww during adsorption process with CMTG-g-PANI/Fe<sub>2</sub>O<sub>3</sub> BNCs. The adsorption/desorption process showed that CMTG-g-PANI/Fe<sub>2</sub>O<sub>3</sub> BNCs could continue to remove AMX after three sequential adsorption/desorption cycles without significantly losing adsorption capacity. The intermolecular interactions such as hydrogen bonding, electrostatic and  $\pi$ - $\pi$  interactions between AMX and CMTG-g-PANI/Fe<sub>2</sub>O<sub>3</sub> BNCs were suggested

for the adsorption mechanism of AMX by CMTG-g-PANI/Fe<sub>2</sub>O<sub>3</sub> BNCs in PI ww during adsorption process.

The AMX removal with adsorption process with CMTG-g-PANI/Fe<sub>2</sub>O<sub>3</sub> BNCs applied to other waste metal ions to prepare the biogenic metals, facilitate their recovery and reuse in degrading micropollutants in PI ww. Finally, the combination of a simple, easy operation preparation process, excellent performance and cost effective, makes this CMTG-g-PANI/Fe<sub>2</sub>O<sub>3</sub> BNCs bioadsorbent a promising option during adsorption process in PI ww treatment.

## 6. Acknowledgement

This research study was undertaken in the Environmental Microbiology Laboratories at Dokuz Eylül University Engineering Faculty Environmental Engineering Department, İzmir, Turkey. The authors would like to thank this body for providing financial support.

## References

1. Idham MF, Abdullah B, Yusof KM. Effects of two cycle heat treatment on the microstructure and hardness of ductile iron. *Pertanika. J. Sci. Technol.* 2017; 25: 99-106.
2. Idham MF, Falyouna O, Eljamal O. Effect of graphene oxide synthesis method on the adsorption performance of pharmaceutical contaminants. *Proc. Int. Exch. Innov. Conf. Eng. Sci.* 2021; 7: 232-9.
3. Arenas NE, Melo VM. Producción pecuaria y emergencia de antibiótico resistencia en Colombia: Revisión sistemática. *Infectio.* 2018; 22: 110-9.
4. Pellerito A, Ameen SM, Micali M, Caruso G. Antimicrobial substances for food packaging products: the current situation. *J AOAC Int.* 2018; 101(4): 942-7.
5. Fridkin S, Baggs J, Fagan R, Magill S, Pollack LA, Malpiedi P, et al. Vital signs: improving antibiotic use among hospitalized patients. *MMWR-Morb. Mortal. Wkly. Rep.* 2014; 63(9): 194-200.
6. Tamma PD, Avdic E, Li DX, Dzintars K, Cosgrove SE. Association of adverse events with antibiotic use in hospitalized patients. *JAMA Intern. Med.* 2017; 177: 1308-15.

7. Huo TI. The first case of multidrug-resistant NDM-1-harboring Enterobacteriaceae in Taiwan: here comes the superbacteria! *J. Chin. Med. Assoc.* 2010; 73: 557-8.
8. Ferri M, Ranucci E, Romagnoli P, Giaccone V. Antimicrobial resistance: A global emerging threat to public health systems. *Crit. Rev. Food Sci.* 2017; 57: 2857-6.
9. Tan L, Li LY, Ashbolt N, Wang XL, Cui YX, Zhu X, et al. Arctic antibiotic resistance gene contamination, a result of anthropogenic activities and natural origin. *Sci. Total Environ.* 2018; 621: 1176-84.
10. Tong S, Pan J, Lu S, Tang J. Patient compliance with antimicrobial drugs: a Chinese survey. *Am. J. Infect. Control.* 2018; 46: E25-9.
11. Alygizakis NA, Gago-Ferrero P, Borova VL, Pavlidou A, Hatzianestis I, et al. Occurrence and spatial distribution of 158 pharmaceuticals, drugs of abuse and related metabolites in offshore seawater. *Sci. Total Environ.* 2016; 541: 1097-105.
12. Casanova LM, Sobsey MD. Antibiotic-resistant enteric bacteria in environmental waters. *Water.* 2016; 8(12): 561-7.
13. Zhang LH, He YW, Chen M, Gao M, Qiu TL, Wang XM. Pollution characteristics of antibiotic resistant bacteria from atmospheric environment of animal feeding operations. *Huan. Jing. Ke. Xue.* 2016; 37: 4531-37.
14. Jiménez-Tototzintle M, Ferreira IJ, da Silva Duque S, Guimarães Barrocas PR, Saggiaro EM. Removal of contaminants of emerging concern (CECs) and antibiotic resistant bacteria in urban wastewater using UVA/TiO<sub>2</sub>/H<sub>2</sub>O<sub>2</sub> photocatalysis. *Chemosphere.* 2018; 210: 449-57.
15. Kerrigan JF, Sandberg KD, Engstrom DR, LaPara TM, Arnold WA. Small and large-scale distribution of four classes of antibiotics in sediment: association with metals and antibiotic resistance genes. *Environ. Sci. Process. Impacts.* 2018; 20: 1167-79.
16. McConnell MM, Truelstrup Hansen L, Jamieson RC, Neudorf KD, Yost CK, Tong A. Removal of antibiotic resistance genes in two tertiary level municipal wastewater treatment plants. *Sci. Total Environ.* 2018; 643: 292-300.
17. Karthikeyan KG, Meyer MT. Occurrence of antibiotics in wastewater treatment facilities in Wisconsin, USA., *Sci. Total Environ.* 2006; 361: 196-207.
18. Dinh QT, Moreau-Guigon E, Labadie P, Alliot F, Teil MJ, Blanchard M, et al. Occurrence of antibiotics in rural catchments. *Chemosphere.* 2017; 168: 483-90.
19. Dong D, Zhang L, Liu S, Guo Z, Hua X. Antibiotics in water and sediments from Liao River in Jilin Province, China: occurrence, distribution, and risk assessment. *Environ. Earth Sci.* 2016; 75(16): 1202.
20. Siedlewicz G, Białk-Bielinska A, Borecka M, Winogradow A, Stepnowski P, Pazdro K. Presence, concentrations and risk assessment of selected antibiotic residues in sediments and near-bottom waters collected from the Polish Coastal Zone in the Southern Baltic Sea-Summary of 3years of studies. *Mar. Pollut. Bull.* 2018; 129: 787-801.
21. Barry S. Dangerously high levels of antibiotics found in world's major rivers, says study. *World news global study, Euronews.* 2019; 1: 1-10.
22. Maycock DS, Watts CD. Pharmaceuticals in drinking water. *Environ. Heal.* 2011; 472-84.
23. Fekadu S, Alemayehu E, Dewil R, Van der Bruggen B. Pharmaceuticals in freshwater aquatic environments: a comparison of the african and european challenge. *Sci. Total Environ.* 2019; 654: 324-37.
24. Wang J, Hao J, Liu D, Qin S, Chen C, Yang C, et al. Flower stamen-like porous boron carbon nitride nanoscrolls for water cleaning. *Nanoscale.* 2017a; 9: 9787-91.
25. Wang X, Wang A, Lu M, Ma J. Synthesis of magnetically recoverable Fe<sub>0</sub>/graphene-TiO<sub>2</sub> nanowires composite for both reduction and photocatalytic oxidation of metronidazole. *Chem. Eng. J.* 2017b; 337: 372-84.
26. Wang W, Zhu Q, Dai Q, Wang X. Fe doped CeO<sub>2</sub> nanosheets for catalytic oxidation of 1,2-dichloroethane: Effect of preparation method. *Chem. Eng. J.* 2017c; 307: 1037-46.
27. Zhu J, Tian M, Zhang Y, Zhang H, Liu J. Fabrication of a novel "loose" nanofiltration membrane by facile blending with Chitosan-Montmorillonite nanosheets for dyes purification. *Chem. Eng. J.* 2015; 265: 184-93.
28. Yang X, Chen Z, Zhao W, Liu C, Qian X, Zhang M, et al. Recent advances in photodegradation of antibiotic residues in water. *Chem. Eng. J.* 2021; 405: 126806.
29. Akyon B, McLaughlin M, Hernández F, Blotvogel J, Bibby K. Characterization and biological removal of organic compounds from hydraulic fracturing produced water. *Environ. Sci. Process.* 2019; 21: 279-90.
30. Zhang C, Li Y, Shuai D, Shen Y, Xiong W, Wang L. Graphitic carbon nitride (g-C<sub>3</sub>N<sub>4</sub>)-based photocatalysts for water disinfection and microbial control: A review. *Chemosphere.* 2019; 214: 462-79.
31. de Souza Santos LV, Meireles AM, Lange LC. Degradation of antibiotics norfloxacin by fenton, UV and UV/H<sub>2</sub>O<sub>2</sub>. *J. Environ. Manag.* 2015; 154: 8-12.
32. Sánchez-Montes I, Fuzer Neto JR, Silva BF, Silva AJ, Aquino JM, Rocha-Filho RC. Evolution of the antibacterial activity and oxidation intermediates during the electrochemical degradation of norfloxacin in a flow cell with a PTFE-doped β-PbO<sub>2</sub> anode: Critical comparison to a BDD anode. *Electrochim. Acta.* 2018; 284: 260-70.
33. Ioannou-Ttofa L, Raj S, Prakash H, Fatta-Kassinos D. Solar photo-fenton oxidation for the removal of ampicillin, total cultivable and resistant E. coli and ecotoxicity from secondary-treated wastewater effluents. *Chem. Eng. J.* 2019; 355: 91-102.
34. Rodríguez-Chueca J, Della Giustina SV, Rocha J, Fernandes T, Pablos C, Encinas Á, et al. Assessment of full-scale tertiary wastewater treatment by UV-C based-AOPs: Removal or persistence of antibiotics and antibiotic resistance genes? *Sci. Total. Environ.* 2019; 652: 1051-61.
35. Alizadeh E, Baseri H. Photocatalytic degradation of sumatriptan succinate by ZnO, Fe doped ZnO and TiO<sub>2</sub>-ZnO nanocatalysts. *Mater. Chem. Horizons.* 2022; 1: 7-21.
36. Alsager OA, Alnajrani MN, Abuelizz HA, Aldaghmani IA. Removal of antibiotics from water and waste milk by ozonation: Kinetics,

- byproducts, and antimicrobial activity. *Ecotoxicol. Environ. Saf.* 2018; 158: 114-22.
37. Cheng D, Ngo HH, Guo W, Liu Y, Chang SW, Nguyen DD, et al. Anaerobic membrane bioreactors for antibiotic wastewater treatment: Performance and membrane fouling issues. *Bioresour. Technol.* 2018; 267: 714-24.
  38. Ghanbari R, Amanat N. Approaches of Membrane Modification for Water Treatment. *Mater. Chem. Horizons.* 2022; 1: 153-67.
  39. Neghi N, Krishnan NR, Kumar M. Analysis of metronidazole removal and micro-toxicity in photolytic systems: Effects of persulfate dosage, anions and reactor operation-mode. *J. Environ. Chem. Eng.* 2018; 6: 754-61.
  40. Tiwari B, Sellamuthu B, Ouarda Y, Drogui P, Tyagi RD, Buelna G. Review on fate and mechanism of removal of pharmaceutical pollutants from wastewater using biological approach. *Bioresour. Technol.* 2017; 224: 1-12.
  41. Nasseh N, Barikbin B, Taghavi L, Nasser MA. Adsorption of metronidazole antibiotic using a new magnetic nanocomposite from simulated wastewater (isotherm, kinetic and thermodynamic studies). *Compos. Part B Eng.* 2019; 159: 146-56.
  42. Mehdizadeh A, Moghadam PN, Ehsanimehr S, Fareghi AR. Preparation of a new magnetic nanocomposite for the removal of dye pollutions from aqueous solutions: Synthesis and characterization. *Mater. Chem. Horizons.* 2022; 1: 23-34.
  43. Movagharnezhad N, Ehsanimehr S, Najafi Moghadam P. Synthesis of Poly (N-vinylpyrrolidone)-grafted-magnetite bromoacetylated cellulose via ATRP for drug delivery. *Mater. Chem. Horizons.* 2022; 1: 89-98.
  44. Akter T, Bañuelos JL, Andrade D, Bañuelos DI, Saupe GB. Rapid adsorption mechanism of methylene blue onto a porous mixed Ti-Nb oxide. *Mater. Chem. Horizons.* 2022; 1: 49-67.
  45. Bebu A, Szabó L, Leopold N, Berindean C, David L. IR, Raman, SERS and DFT study of amoxicillin. *J. Mol. Struct.* 2011; 993: 52-6.
  46. Maichin F, Freitas LC, Ortiz N. The use of converter slag—magnetite to decompose amoxicillin by fenton oxidation process. *Orbital. Electron. J. Chem.* 2013; 5: 213-7.
  47. Mohammadi A, Kazemipour M, Ranjbar H, Walker RB, Ansari M. Amoxicillin removal from aqueous media using multi-walled carbon nanotubes. *Fuller. Nanotub. Carbon Nanostruct.* 2015; 23: 165-9.
  48. Andreozzi R, Canterino M, Marotta R, Paxeus N. Antibiotic removal from wastewaters: The ozonation of amoxicillin. *J. Hazard. Mater.* 2005; 122: 243-50.
  49. Pezoti O, Cazetta AL, Bedin KC, Souza LS, Martins AC, Silva TL, et al. NaOH-activated carbon of high surface area produced from guava seeds as a high-efficiency adsorbent for amoxicillin removal: Kinetic, isotherm and thermodynamic studies. *Chem. Eng. J.* 2016; 288: 778-88.
  50. Boukhelkhal A, Benkortbi O, Hamadeche M, Hanini S, Amrane A. Removal of amoxicillin antibiotic from aqueous solution using an anionic surfactant. *Water Air Soil Pollut.* 2015; 226: 323-34.
  51. Sopaj F, Rodrigo MA, Oturan N, Podvorica FI, Pinson J, Oturan MA. Influence of the anode materials on the electrochemical oxidation efficiency. Application to oxidative degradation of the pharmaceutical amoxicillin. *Chem. Eng. J.* 2015; 262: 286-94.
  52. Kıdak R, Dogan S. Medium-high frequency ultrasound and ozone based advanced oxidation for amoxicillin removal in water. *Ultrasound. Sonochem.* 2018; 40: 131-9.
  53. Belaissa Y, Nibou D, Assadi AA, Bellal B, Trari M. A new hetero-junction p -CuO/ n -ZnO for the removal of amoxicillin by photocatalysis under solar irradiation. *J. Taiwan. Inst. Chem. Eng.* 2016; 68: 254-65.
  54. de Franco MAE, de Carvalho CB, Bonetto MM, de Pelegrini Soares R, Feris LA. Removal of amoxicillin from water by adsorption onto activated carbon in batch process and fixed bed column: kinetics, isotherms, experimental design and breakthrough curves modelling. *J. Clean. Prod.* 2017; 161: 947-56.
  55. Moradi SE. Highly efficient removal of amoxicillin from water by magnetic graphene oxide adsorbent. *Chem. Bull. 'POLITEHNICA' Univ. Timisoara.* 2015; 60(74)2: 41-8.
  56. Kerkez-Kuyumcu O, Bayazit SS, Salam MA. Antibiotic amoxicillin removal from aqueous solution using magnetically modified graphene nanoplatelets. *J. Ind. Eng. Chem.* 2016; 36: 198-205.
  57. Balarak D, Mahdavi Y, Maleki A, Daraei H, Sadeghi S, Br. Studies on the Removal of Amoxicillin by Single Walled Carbon Nanotubes. *J. Pharmaceut. Res.* 2016; 10(4): 1-9.
  58. Fazelirad H, Ranjbar M, Taher MA, Sargazi G. Preparation of magnetic multi-walled carbon nanotubes for an efficient adsorption and spectrophotometric determination of amoxicillin. *J. Ind. Eng. Chem.* 2015; 21: 889-92.
  59. Kakavandi B, Esrafil A, Mohseni-Bandpi A, Jafari AJ, Kalantary RR. Magnetic Fe<sub>3</sub>O<sub>4</sub>@C nanoparticles as adsorbents for removal of amoxicillin from aqueous solution. *Water Sci. Technol.* 2014; 69(1): 147-55.
  60. Saucier C, Karthickeyan P, Ranjithkumar V, Lima EC, dos Reis GS, de Brum IA. *Environ. Sci. Pollut. Res.* 2017; 24(6): 5918-32.
  61. Alsbaiee A, Smith BJ, Xiao L, Ling Y, Helbling DE, Dichtel WR. Rapid removal of organic micropollutants from water by a porous  $\beta$ -cyclodextrin polymer. *Nature.* 2016; 529: 190-4.
  62. Imanipoor J, Mohammadi M, Dinari M, Ehsani MR. Adsorption and desorption of amoxicillin antibiotic from water matrices using an effective and recyclable MIL-53 (Al) metal-organic framework adsorbent. *J. Chem. Eng. Data.* 2020; 66: 389-403.
  63. Moussavi G, Alahabadi A, Yaghmaeian K, Eskandari M. Preparation, characterization and adsorption potential of the NH<sub>4</sub>Cl-induced activated carbon for the removal of amoxicillin antibiotic from water. *Chem. Eng. J.* 2013; 217: 119-28.
  64. Ali I, Afshinb S, Poureshgh Y, Azari A, Rashtbari Y, Feizizadeh A, et al. Green preparation of activated carbon from pomegranate peel coated with zero-valent iron nanoparticles (nZVI) and isotherm and kinetic studies of amoxicillin removal in water. *Environ. Sci. Pollut. Res.* 2020; 27: 36732-43.

65. Chakhtouna H, Benzeid H, Zari N, Bouhfid R. Functional CoFe<sub>2</sub>O<sub>4</sub>-modified biochar derived from banana pseudostem as an efficient adsorbent for the removal of amoxicillin from water. *Sep. Purif. Technol.* 2021; 266: 118592.
66. Taghavizadeh Yazdi ME, Nazarnezhad S, Mousavi SH, Sadegh Amiri M, Darroudi M, Bairo F, et al. Gum tragacanth (GT): A versatile biocompatible material beyond borders. *Molecules.* 2021; 26(6): 1510: 1-18.
67. Verbeken D, Dierckx S, Dewettinck K. Exudate gums: occurrence, production, and applications. *Appl. Microbiol. Biotechnol.* 2003; 63: 10-21.
68. Tischer CA, Iacomini M, Gorin PAJ. Structure of the arabinogalactan from gum tragacanth (*Astragalus gummifer*). *Carbohydr. Res.* 2002; 337: 1647-55.
69. Nejatian M, Abbasi S, Azarikia F. Gum tragacanth: structure, characteristics and applications in foods. *Int. J. Biol. Macromol.* 2020; 160: 846-60.
70. Nussinovitch A. Miscellaneous uses of plant exudates. *Plant gum exudates of the world: Sources, distribution, properties and applications.* Boca Raton, USA: CRC Press. 2010; 347-68.
71. Kora A.J, Arunachalam J. Green fabrication of silver nanoparticles by gum tragacanth (*Astragalus gummifer*): A dual functional reductant and stabilizer. *J Nanomater.* 2012; 2012: 869765.
72. Ranjbar-Mohammadi M, Bahrami SH, Joghataei MT. Fabrication of novel nanofiber scaffolds from gum tragacanth/ poly(vinyl alcohol) for wound dressing application: In vitro evaluation and antibacterial properties. *Mater. Sci. Eng. C.* 2013; 33(8): 4935-43.
73. Padil VVT, Waclawek S, Černík M, Varma RS. Tree gum-based renewable materials: Sustainable applications in nanotechnology, biomedical and environmental fields. *Biotechnol. Adv.* 2018; 36(7): 1984-2016.
74. Kora AJ. Plant arabinogalactan gum synthesized palladium nanoparticles: Characterization and properties. *J. Inorg. Organomet. Polym. Mater.* 2019; 29(6): 2054-63.
75. Kora A.J. Exudate tree gums: Properties and applications. In Inamuddin, Ahamed MI, Boddula R, Altalhi T, editors. *Polysaccharides*; Hoboken, NJ: John Wiley & Sons. Inc. 2021; 205-220.
76. Boamah PO, Afoakwah NA, Onumah J, Osei ED, Mahunu GK. Physicochemical properties, biological properties and applications of gum tragacanth-A review. *Carbohydr Polym Technol Appl.* 2023; 5: 100288.
77. Zare EN, Makvandi P, Tay FR. Recent progress in the industrial and biomedical applications of tragacanth gum: A review. *Carbohydr. Polym.* 2019; 212: 450-67.
78. Ansari MJ, Rehman NU, Ibnouf E, Alalaiwe A, Ganaie MA, Zafar A. Gum acacia- and gum tragacanth-coated silver nanoparticles: synthesis, physiological stability, in-vitro, ex-vivo and in-vivo activity evaluations. *Coatings.* 2022; 12(10): 1579.
79. Shan D, Deng S, Zhao T, Wang B, Wang Y, Huang J, et al. Preparation of ultrafine magnetic biochar and activated carbon for pharmaceutical adsorption and subsequent degradation by ball milling. *J. Hazard. Mater.* 2016; 305: 156-63.
80. Abdollahi Z, Zare EN, Salimi F, Goudarzi I, Tay FR, Makvandi P. Bioactive carboxymethyl starch-based hydrogels decorated with CuO nanoparticles: Antioxidant and antimicrobial properties and accelerated wound healing in vivo. *Int. J. Mol. Sci.* 2021; 22: 2531.
81. Sudhakara K, Kumar AP, Kumara BP, Raghavendera A, Ravia S, Kenie DN, et al. Synthesis of  $\gamma$ -Fe<sub>2</sub>O<sub>3</sub> nanoparticles and catalytic activity of azide-alkyne cycloaddition reactions. *Asian J. Nanosci. Mater.* 2018; 1: 172-82.
82. Dubinin MM. In *Progress in Membrane and Surface Science* (Edited by D. A. Cadenhead). Academic Press, New York, USA. 1975; 9: 1.
83. Hassanzadeh-Afruzi F, Heidari G, Maleki A. Magnetic Nanocomposite Hydrogel based on Arabic Gum for Remediation of Lead(II) from Contaminated Water. *Mater. Chem. Horizons.* 2022; 1: 107-22.
84. Lipps WC, Braun-Howland EB, Baxter TE. *Standard Methods for the Examination of Water and Wastewater.* (24th. Edition). Lipps, W.C., Braun-Howland, E.B., Baxter, T.E. (editors), American Public Health Association (APHA), American Water Works Association (AWWA), Water Environment Federation (WEF), Elevate Your Standards. American Public Health Association 800 I Street, NW Washington DC: 20001-3770, USA, 2022.
85. Olthof M, Eckenfelder WW. Coagulation of textile wastewater. *Text. Chem. Color.* 1976; 8: 18-22.
86. Eckenfelder WW. *Industrial Water Pollution Control* (2nd ed), Signapore: McGraw-Hill Inc. 1989.
87. Zar JH. *Biostatistical analysis*, Prentice-Hall, Englewood Cliffs. 1984.
88. Statgraphics Centurion XV, software, StatPoint Inc, Statgraphics Centurion XV, Herndon, VA, USA, 2005.
89. Behrouzi M, Moghadam PN. Synthesis of a new superabsorbent copolymer based on acrylic acid grafted onto carboxymethyl tragacanth. *Carbohydr. Polym.* 2018; 202: 227-35.
90. Bachra Y, Grouli A, Damiri F, Talbi M, Berrada M. A Novel superabsorbent polymer from crosslinked carboxymethyl tragacanth gum with glutaraldehyde: synthesis, characterization, and swelling properties. *Int. J. Biomater.* 2021; 2021: 5008833.
91. Van Cuong N, Hieu TQ, Thien PT, Vu LD, Van Tan L. Reusable starch-graft-polyaniline/Fe<sub>3</sub>O<sub>4</sub> composite for removal of textile dyes. *Rasayan J. Chem.* 2017; 10: 1446-54.